LETTER OF INTENT
for RIBF PAC June 2014

OEDO* Project

Susumu Shimoura for OEDO Collaboration†

Center for Nuclear Study (CNS), the University of Tokyo

Abstract

We propose construction of an energy-degrading system consisting of a RF deflector with two STQ's after a mono-energetic degrader in the SHARAQ beam line. The RF deflector acts as a focusing element for a secondary beam after a mono-energetic degrader, which provides a reasonably small beam size less than 2 cm (FWHM) even for energies less than 10A MeV.

1 Physics subjects to be investigated

1.1 Motivation

The RIBF have been providing intense RI beam in wide area in the nuclear chart via the BigRIPS separator[1, 2]. So far, major in-beam studies at the RIBF are restricted to the energy region more than 200 A MeV. This energy region is unique and suitable for studies by using impulse interaction such as inelastic, charge exchange, and knockout reactions, which mainly provide information on ground states, low-excited states and impulse response of exotic nuclei. On the other hand, low-energy nuclear reactions with energies compatible with or below the Fermi momentum in nuclei have additional kinds of aspects on the studies of nuclear structure and nuclear dynamics, since nucleon, cluster and angular momenta as well as energies can be transferred to nuclear systems.

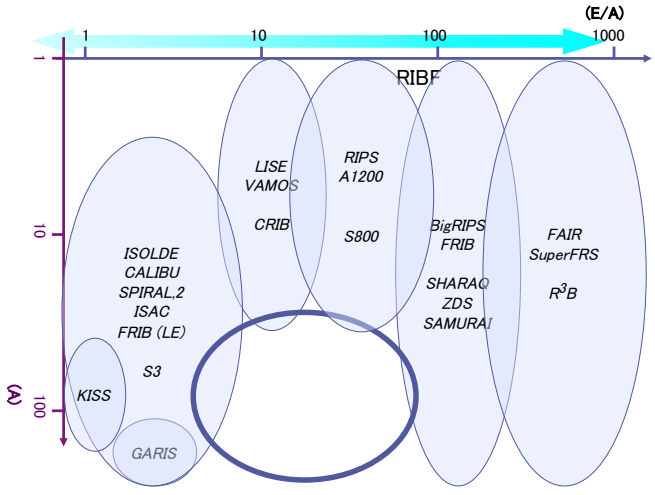

Figure 1: Territory of major RI-beam Facilities on the map of the incident-energy versus mass.

*Optimized Energy Degrading Optics for RI beam: 大江戸

†Shin'ichiro Michimasa, Kentaro Yako, Hidetoshi Yamaguchi, Shinsuke Ota, Masafumi Matsushita, Eiji Ideguchi (RCNP), Kazunari Yamada (RNC)

Figure 1 shows a map of several RI beam facilities (separators and spectrometers; operating and future) on the incident energy versus mass number plane. We can find untouched region of 5 to 100 A MeV for $A > 50$. This region is too high energy for acceleration from ISOL, too heavy for fragmentation facilities below 100 A MeV, and too low energy for facilities more than 300 A MeV.

The easiest way to approach this blank region seems to be energy degrading method from high-energy RI beams. However, there are still inevitable difficulties in degrading procedure, which causes large image sizes and energy spreads due to increase of phase spaces, charge-state distribution, and contaminants if the beam, as shown in subsect. 2.1. For example, Ref. [3] proposes a reasonable energy-degrading scheme by manipulating positions and shapes of degraders, and is estimated to achieve a 10-cm image size for mass-100 nuclei with a few A MeV. Since it is obvious that the smaller image size is the better for experimental opportunities, we propose a new scheme of beam line by using RF structure of a beam from the cyclotrons of RIBF.

1.2 Expected physics programs

The followings are examples of physics programs for exotic nuclei:

- Nucleon transfer reactions (10 – 50 A MeV)
  Evolution of shell structure seen in unoccupied orbitals are studied by single-particle states populated by (d,p) and (d,n) reactions below 20 A MeV. Cross sections of nucleon transfer also provide information on neutron/proton capture cross section via the asymptotic normalization constants (ANC).
  For orbitals with higher angular momenta are studies by (α,t), (α,^{3}He) reactions at 30–50 A MeV.

- Pair transfer / Cluster transfer (10 – 20 A MeV)
  Di-neutron pickup reactions such as (p,t) provide us information on di-neutron correlation in nuclei especially for very neutron-rich region where BCS-BEC cross-over is predicted.
  Cluster transfer reactions, such as (^{6}Li,d), (^{7}Li,p) and so on, are expected to populate excited cluster states in neutron-rich nuclei, where new degrees-of-freedom from weakly bound neutrons may affect clustering such as glue-effects, interplay between molecular and atomic orbitals, deformation in mean fields, and so on.

- Deep inelastic collisions (incomplete fusion) (5 – 30 A MeV)
  Fusion reaction ($\sim$ 5 A MeV)
  Dynamics of dissipating reactions of exotic nuclei is interested as leading candidates of synthesizing methods heavy-mass nuclei, various kinds of deformed states with high-spin, and so on. Use of unstable nuclei provides opportunities to control reaction Q-values, excitation energies of compound system, maximum angular momenta by changing combination of reactions.

- Coulomb excitation reactions for low-energy γ-rays ($\sim$ 50 A MeV)
  In-beam spectroscopy using inelastic scattering at high incident energies above 100 A MeV suffers from huge backgrounds of low-energy photons from atomic processes, which limits the gamma-ray energies above several hundreds of keV. Beams at 50A MeV or less enable us to measure Coulomb excitation for highly deformed neutron-rich nuclei.

2 Design

2.1 Basic idea

We consider the phase space of ion optics by horizontal (x and θ) and momentum ($\delta(=\delta p/p_0)$) degree-of-freedom in the vertically symmetric beam line. (vertical degree-of-freedoms (y and ϕ) are decoupled from the others.) Profiles of ions in a beam line consisting of static ion-optical devices are characterized by the shape of the phase space in the 3-dimensional space of x, θ, and δ.

At the production target, the stronger the intensities of RI beams are obtained by the larger the acceptances in θ- and $\delta(=\delta p/p_0)$-axes. ($\Delta\theta = \pm 40$mr and $\Delta\delta = \pm 3\%$ for BigRIPS) Initial phase-space volume is determined by the acceptances and the small size x of the primary beam. It is noted that only one degree-of-freedom (x) has small size. Since phase-space volume is inversely proportional to p_0, degrading energy makes the phase-space volume larger and larger. Additional enlargement occurs due to energy straggling in degraders. Degrading beam energy from 300 A MeV to 3 A MeV, phase-space volume increases much more than 10 times. Higher order aberrations also become significant for such large phase-space volume.

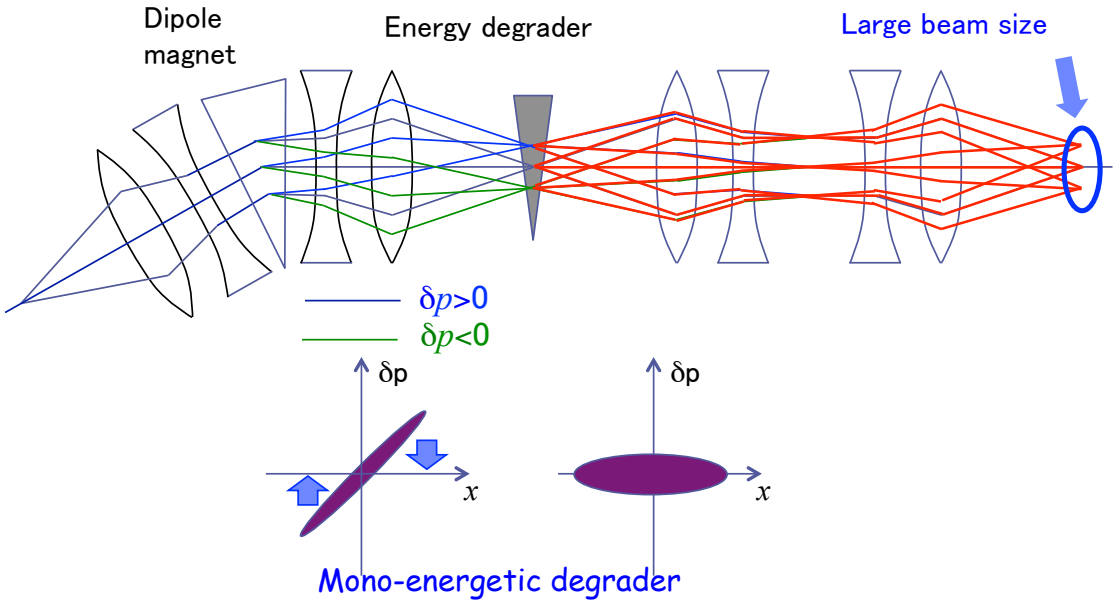

Figure 2: Schematic optics of beam line with mono-energetic degrader.

As a simple example, we examine optics with mono-energetic degrader. Figure 2 schematically shows the optics as well as the phase space in x vs δp. A wedge-shaped degrader at dispersive focus acts as both degrading energy and compressing energy spread. However, after the degrader the beam size (x) becomes large and cannot be focus by static optical devices. The reducing factor of the energy spread is the same as enlargement factor of the beam size (x) at achromatic focus.

The difficulty can be solved by introducing another degree-of-freedom, t, which is conjugate to δ. Fortunately, the primary beam at RIBF is produced by the cyclotron having RF structure. All the produced RI has the same RF structure at the production target. Because of velocity spread, the arrival time (t) of a beam particle at a dispersive focus depends on its horizontal position (x): higher (lower) momentum corresponds to earlier (later) timing. As shown in Fig. 3, an RF

deflector placed in the point-to-parallel position kicks beam particles back by means of timing so as to focus the beam.

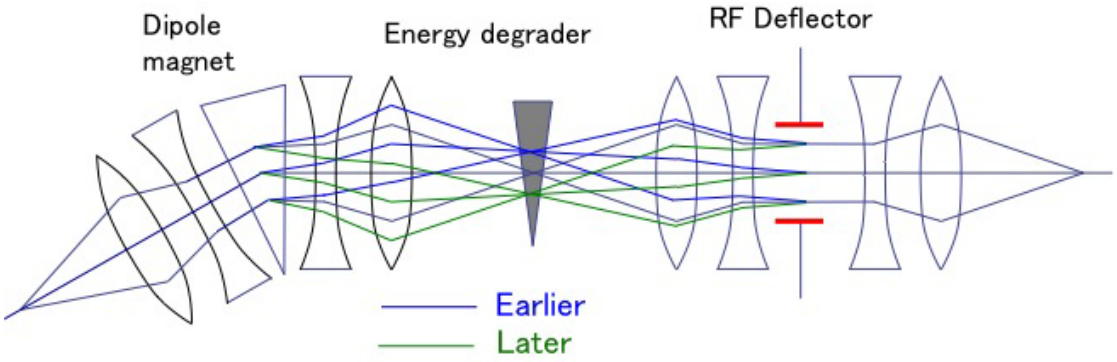

Figure 3: Beam optics with mono-energetic degrader and RF deflector.

As shown in Appendix A, the beam profiles can be described systematically under consideration of four degrees of freedom. It is noted that the initial momentum spread (δ) is swapped to the timing spread (t) with little changes in the other degree-of-freedoms.

2.2 Experimental Devices and Their Specification

The specification of the RF deflector is considered by the experience in the presently used RF deflector at the RIPS facility in RIKEN[4], which is a vertically kick system for purification of RI beams. The proposed RF deflector is operated after energy degrading to about 50 A MeV, which is almost same as the RIPS facility. Assuming scalability, our design of the new RF deflector is about twice in size in order to increase acceptances and quality. The specifications are refined based on the simulations shown in Sect. 3 as follows:

Frequency	17.6 ± 1.5 MHz
Maximum voltage	300 kV
Gap between electrodes	200 mm
Length of electrodes	1000 mm
Width of electrodes	400 mm
Vacuum	5×10^{-6} Pa

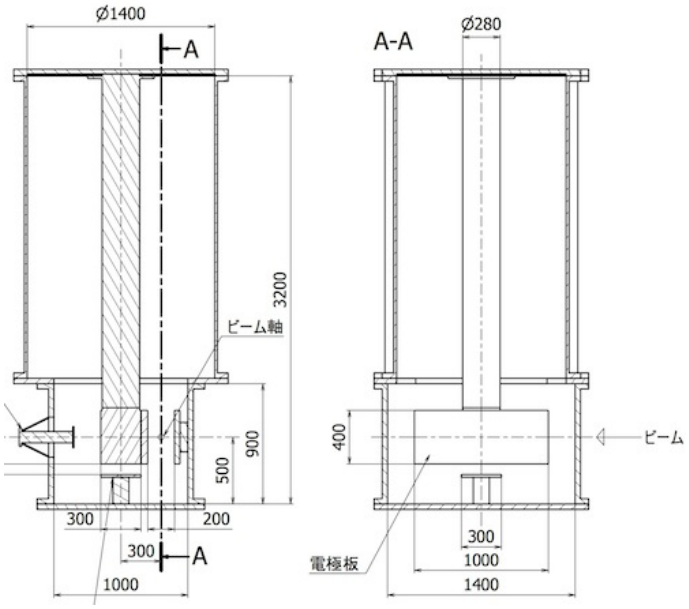

The quadrupole magnets are planed to be the same superconducting triplet Q's (STQ) as those in the BigRIPS facility.

2.3 Envisaged site in RIBF

Among possible sites for the OEDO system in the RIBF, we decided to construct it in the SHARAQ beam line[5] under the following consideration:

- There should be a suitable dispersive focal plane before an enough length of straight line, which is satisfied by the FH8 focus in the SHARAQ beam line satisfies.
- The height of the roof should be enough for the size of the RF cavity (about 4m).
- Some possible physics programs require a spectrometer for charged particles. The first part (QQD) of the SHARAQ can be used for a broad-range magnetic spectrometer. It is noted that the SHARAQ is rotatable unto 15°.

Figure 4 shows our conceptual design of the beam line. Two STQ's and RF deflector are placed in the E20 experimental room.

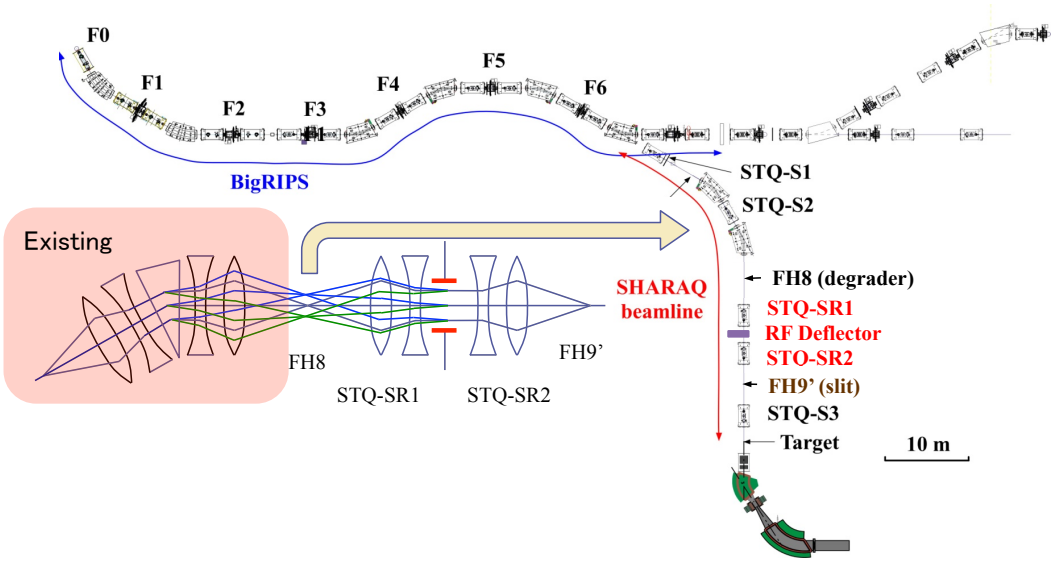

Figure 4: Design of Beamline.

Based on the above scheme and design, we call the new project as OEDO (**O**ptimized **E**nergy **D**egrading **O**ptics for RI beam: **大江戸**, which is the old name of the Tokyo metropolitan area).

3 Simulation

Actual performance of the OEDO is going to examine by simulation. Here, we present some results mainly based on first order calculations.

Figure 5 schematically shows the condition of the simulation as a typical case. A ^{132}Sn beam produced by in-flight fission of ^{238}U at 345 A MeV. As usual SHARAQ/BigRIPS scheme, the starting condition is ^{132}Sn with 250 A MeV ($\delta = \pm 2\%$, $\Delta\theta = \pm 10$mr, $\Delta\phi = \pm 30$mr). Two stage degrading scheme is considered. The ^{132}Sn beam of 50 A MeV is produced by a mono-energetic

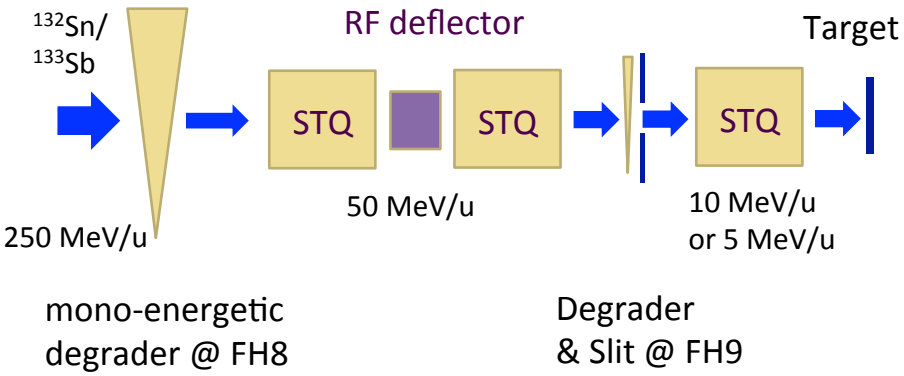

Figure 5: Energy degrading scheme in the simulation.

degrader at FH8 (first stage) and is transported to the RF deflector. The RF deflector kicks beams by means of timing to focus the beam at FH9. The energy of ^{132}Sn is slowed down to 10 or 5 A MeV by another degrader at FH9. Figure 6 shows the beam profiles in the foci (FH8, FH9 and Target) with RF and without RF. As seen in the left panel, the beam image at FH9 with RF is much smaller than that without RF. In addition, it is seen a correlation between energy and position (dispersion). This is produced by finite image size for the same δ at FH8, *i.e.* the ions with the same momentum and different position pass through different thickness of the wedge degrader at FH8. By means of this dispersion, we can use wedge-type degrader for the second stage, which again compress momentum spread for low-energy beam.

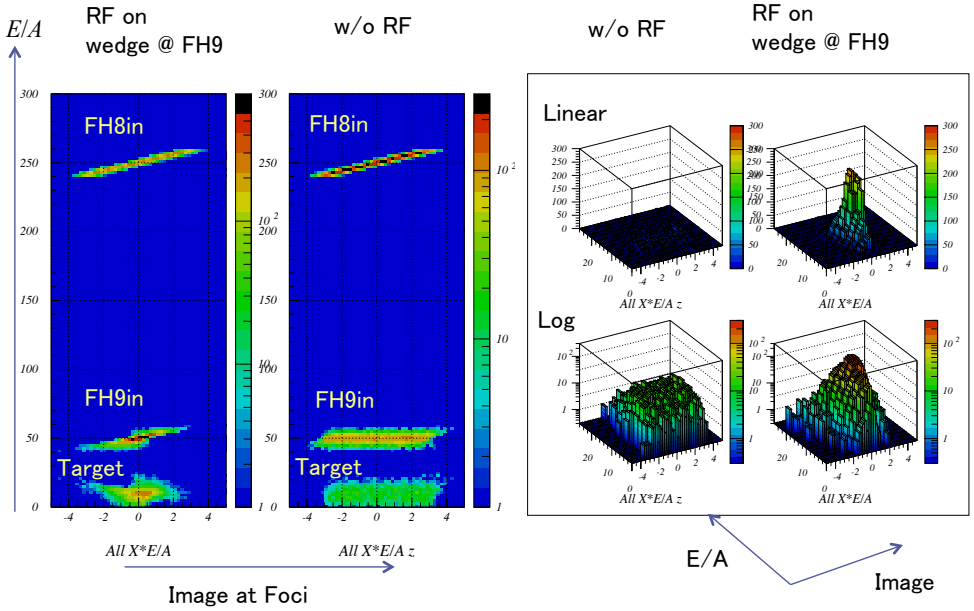

Figure 6: Left: Beam energy as a function of position (x (cm)) at the foci (FH8, FH9 and Target) with RF and without RF. Right: two-dimensional Lego plot as functions of position and energy in linear/log scale for without RF and with RF. The second degrader is set to the final energy of 10 A MeV.

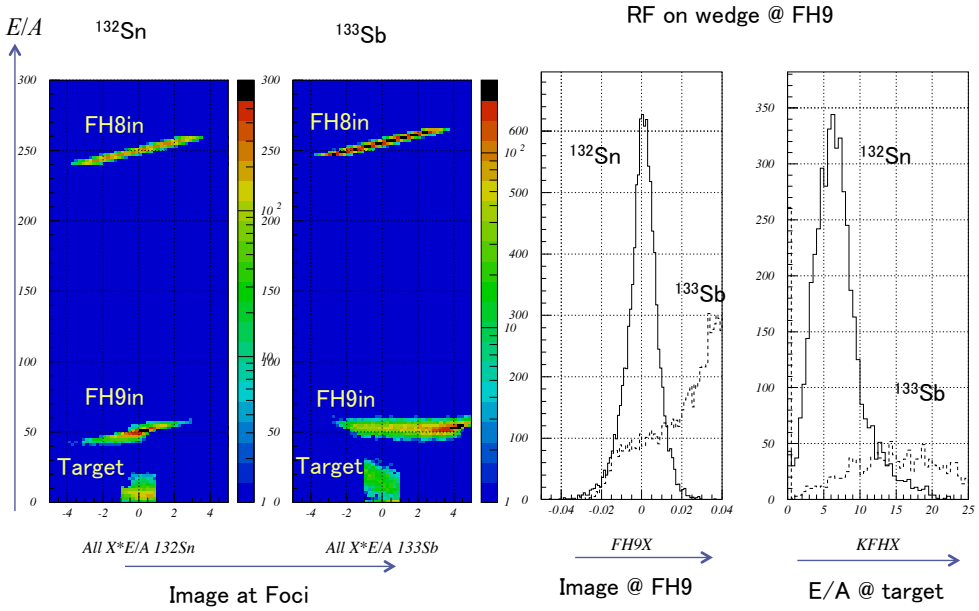

Figure 7: Left: Beam energy as a function of position (x (cm)) at the foci (FH8, FH9 and Target) for ^{132}Sn and ^{133}Sb. A slit of $\pm$1cm is used at FH9. Right: Image and energy distributions at the target for ^{132}Sn and ^{133}Sb. The second degrader is set to the final energy of 6 A MeV.

As an example of contaminants, ^{133}Sb with the same rigidity is examined in the simulation (Fig. 7). Because of slightly different velocity of ^{133}Sb from ^{132}Sn with the same rigidity, its arrival timing to the RF deflector mismatches the focusing phase. Figure 7 clearly shows phase mismatch. Consequently, the portion of ^{132}Sn increases by using the slit at FH9.

Since the energy spread after the final energy degrading is large, higher order aberration is expected to make the beam size larger. The main contributions are $(x|\theta\delta)$ and $(y|\phi\delta)$ due to the momentum dependence of focusing power of quadrupole magnets.

Study of charge state is also important. In the present simulation we assume $q = 50$ for ^{132}Sn in spite of the fact that optimum q at 50 A MeV is 49 for ^{132}Sn. Difference in rigidity of 2 % requires 2 % increase of the voltage of the RF deflector. It is noted that because of no deflection for the central-timing ion in the RF deflector, ions with central-timing but different q ($\delta \neq 0$) are transported to the focus (FH9): $(x|\delta)$=0. This fact also indicate that the charge state distribution can be considered to be higher-order effects such as $(x|\theta\delta)$, which are mainly produced by quadrupole magnets between FH9 and Target.

The charge distribution of low-energy ion after the second degrader also be treated by means of the variation of δ. Simulation with such higher order effects including charge distributions is still on going.

4 Costs

Depending on the financial situation, rough estimations for construction except for performing actual physics experiments are follows:

RF deflector	150 M yen
STQ × 2	300 M yen
Beam line devices	50 M yen
Total	500 M yen

5 Other remarks

Because of large acceptance and deflecting power, proposed new STQ's are useful for the standard SHARAQ operation with dispersion-matching and other modes. They are also expected to make acceptance large for the beam transport to the Rare RI Ring.

Gamma-ray spectroscopy with future Ge array such as CAGRA or GRETINA will be very productive in the OEDO project.

References

[1] T. Kubo, *Nucl. Instrum. Meth. in Phys. Res.* **B204**, 97 (2003)

[2] T. Kubo, et al., *Prog. Theor. Exp. Phys.* **2012** (2012) 03C003

[3] E. Ideguchi, *Prog. Theor. Exp. Phys.* **2012** (2012) 03C005

[4] K. Yamada, T. Motobayashi, and I. Tanihata, *Nucl. Phys. A* **746** (2004) 156c

[5] T. Uesaka, et al., *Prog. Theor. Exp. Phys.* **2012** (2012) 03C007

A Phase spaces in four degrees of freedom

Figure 8(A) shows the beam profile at the production target. Both the sized in x and t are small, whereas the others are large. At the dispersive focus, not only δ but also t depend on the position x, since finite flights with different velocities makes spread in time (Fig. 8(B)). A point-to-parallel transport using triplet Q-magnet switches the position (x) and angle (θ) ((C) to (D); (E) to (F) in Fig. 8). The RF deflector changes the angle (θ) depends on timing (t) (Fig. 8(D)). It is noted that the initial momentum spread in (A) is swapped to the timing spread in (F) with little changes in the other degree-of-freedoms.

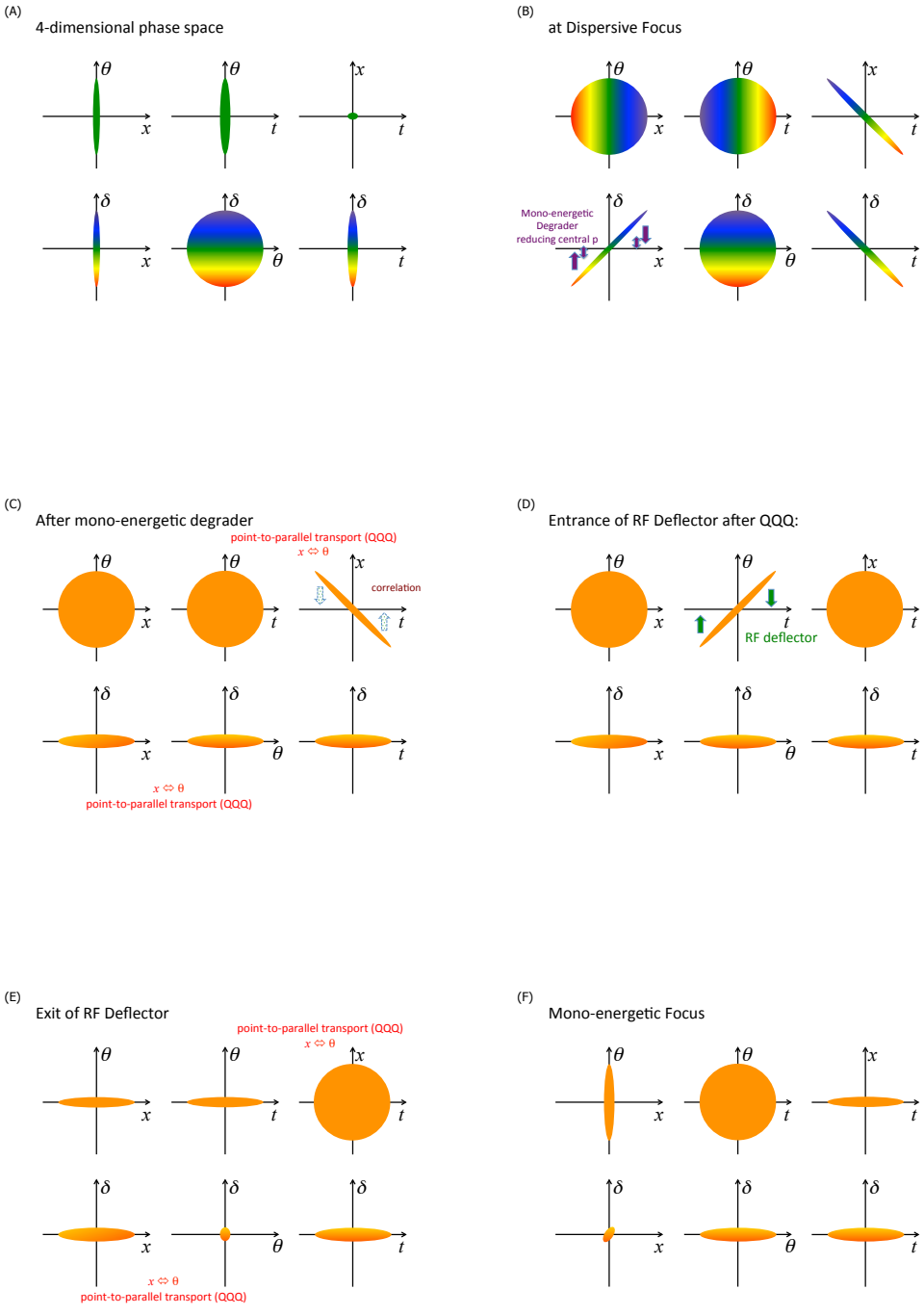

Figure 8: Shapes of beam profiles in the four-dimentional phase space. (A) at production target, (B) at dispersive focus, (C) after mono-energetic degrader at dispersive focus, (D) at entrance of RF deflector, (E) at exit of RF deflector, (F) at mono-energetic focus.